ACS OMEGA

http://pubs.acs.org/journal/acsodf

Article

Novel [^{111}In]In-BnDTPA-EphA2-230-1 Antibody for Single-Photon Emission Computed Tomography Imaging Tracer Targeting of EphA2

Takenori Furukawa, Hiroyuki Kimura,* Minon Sasaki, Takumu Yamada, Takumi Iwasawa, Yusuke Yagi, Kazunori Kato, and Hiroyuki Yasui

Cite This: *ACS Omega* 2023, 8, 7030−7035

Read Online

ACCESS | Metrics & More | Article Recommendations | Supporting Information

ABSTRACT: Erythropoietin-producing hepatocellular receptor A2 (EphA2) is overexpressed in cancer cells and causes abnormal cell proliferation. Therefore, it has attracted attention as a target for diagnostic agents. In this study, the EphA2-230-1 monoclonal antibody (EphA2-230-1) was labeled with [^{111}In]In and evaluated as an imaging tracer for single-photon emission computed tomography (SPECT) of EphA2. EphA2-230-1 was conjugated with 2-(4-isothiocyanatobenzyl)-diethylenetriaminepentaacetic acid (p-SCN-BnDTPA) and then labeled with [^{111}In]In. [^{111}In]In-BnDTPA-EphA2-230-1 was evaluated in cell-binding, biodistribution, and SPECT/computed tomography (CT) studies. The cellular uptake ratio of [^{111}In]In-BnDTPA-EphA2-230-1 was 14.0 ± 2.1%/mg protein at 4 h in the cell-binding study. In the biodistribution study, a high uptake of [^{111}In]In-BnDTPA-EphA2-230-1 was observed in tumor tissue (14.6 ± 3.2% injected dose/g at 72 h). The superior accumulation of [^{111}In]In-BnDTPA-EphA2-230-1 in tumors was also confirmed using SPECT/CT. Therefore, [^{111}In]In-BnDTPA-EphA2-230-1 has potential as a SPECT imaging tracer for EphA2.

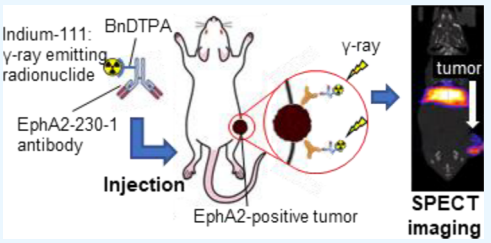

1. INTRODUCTION

Erythropoietin-producing hepatocellular (Eph) receptors are known as the largest tyrosine kinase receptor family, and 14 subtypes have been confirmed in the human genome. These 14 subtypes are classified into nine EphA and five EphB subclasses.[1,2] Eph receptors and their ephrin ligands are bound to cell membranes, and their binding causes dimerization and subsequent activation.[3,4] Additionally, Eph receptors are involved in cell proliferation and survival, and by controlling their activation, Eph receptors can inhibit the proliferation and migration of cancer cells. However, some Eph receptors are overexpressed in cancer cells and activate without binding to ephrin, causing abnormal cell proliferation.[5,6] Among them, erythropoietin-producing hepatocellular receptor A2 (EphA2) is particularly overexpressed in cancer cells, including breast and prostate cancer and malignant gliomas.[7−9] The relationship between tumor malignancy and EphA2 has also been described.[10,11] For example, the expression level of EphA2 has been reported to increase with malignancy in breast cancer patients. Moreover, EphA2 expression and the survival rate of breast cancer patients are correlated,[12] indicating that EphA2 can be used as a therapeutic target; therefore, small molecule compounds, peptides, and antibodies have been developed to target EphA2.[13−15] Although three clinical trials have been conducted for therapeutic agents, none of the small molecule compounds have been approved for treatment.[9] In contrast, research on antibodies targeting EphA2 has progressed since 2007.[16] Several antibodies have been studied,[17−20] including DS-8895a, which has been evaluated in clinical trials.[21] Through pharmacokinetics, DS-8895a labeled with [^{111}In]In has been found to have poor clearance from blood, with a low tumor-to-blood ratio of 0.94 at 7 days.[19] A low tumor-to-blood ratio may result in unclear tumor images. Therefore, the aim of this study was to develop a novel antibody imaging tracer targeting EphA2 to improve the tumor-to-blood ratio. Our novel monoclonal antibody that targets EphA2 was evaluated in vitro through a cell-binding study and in vivo through biodistribution and single-photon emission computed tomography/computed tomography (SPECT/CT) studies.

2. RESULTS AND DISCUSSION

2.1. DTPA Conjugates with the Antibody. We used the EphA2-230-1 monoclonal antibody (EphA2-230-1) as the antibody that specifically binds to EphA2.[22] This antibody was constructed using a previously reported method.[23] Moreover, diethylenetriamine pentaacetic acid (DTPA), which is necessary for complex formation with [^{111}In]In, by random

Received: December 9, 2022
Accepted: January 26, 2023
Published: February 9, 2023

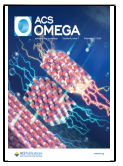

https://doi.org/10.1021/acsomega.2c07849
ACS Omega 2023, 8, 7030−7035

modification to a lysine residue was introduced into EphA2-230-1. [^{111}In]In is a radionuclide that is also used in clinical practice for SPECT imaging. Additionally, DTPA is a chelating agent with the highest binding affinity for In. The molecular weight of the EphA2-230-1 antibody reacted with 2-(4-isothiocyanatobenzyl)-diethylenetriaminepentaacetic acid (*p*-SCN-BnDTPA) (BnDTPA-EphA2-230-1) was measured using matrix-assisted laser desorption/ionization time-of-flight mass spectrometry (MALDI-TOF-MS) (Bruker, Billerica, MA, USA) and found to be 154670.7 *m/z* (Figure S1). The molecular weight of the EphA2-230-1 antibody was 147351.5 *m/z*; for that reason, an average of 13.4 DTPAs was introduced per EphA2-230-1.

2.2. Binding Affinity for EphA2. The binding of EphA2-230-1, BnDTPA-EphA2-230-1, and natIn-labeled BnDTPA-EphA2-230-1 (natIn-BnDTPA-EphA2-230-1) to EphA2 was examined using flow cytometry. These antibodies were bound to EphA2-positive U87MG cells[24] in a dose-dependent manner. As shown in Figure 1, the reactivity of BnDTPA-

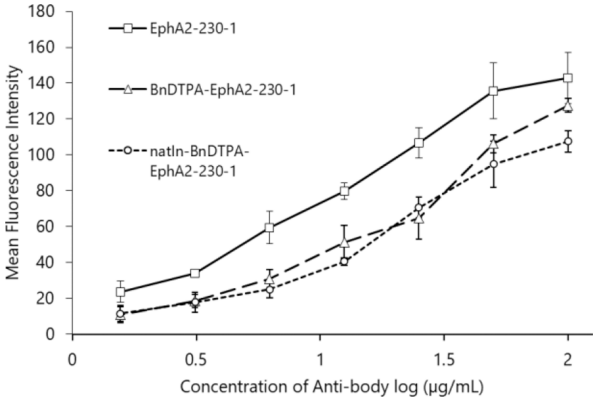

Figure 1. EphA2-230-1, BnDTPA-EphA2-230-1, and natIn-BnDTPA-EphA2-230-1 were found to bind at similar levels to EphA2 in U87MG cells.

and natIn-BnDTPA-EphA2-230-1 was slightly weaker than that of intact EphA2-230-1 (equilibrium dissociation constant: EphA2-230-1 = 128.9 nM, BnDTPA-EphA2-230-1 = 401.8 nM, natIn-BnDTPA-EphA2-230-1 = 529.5 nM), indicating that conjugated DTPA might interfere with the binding site of EphA2-230-1. Nevertheless, BnDTPA- and natIn-BnDTPA-EphA2-230-1 retained sufficient binding to EphA2. In the future, it is necessary to control the number and position of BnDTPA molecules introduced into the antibody. Furthermore, combinations of different ligands and nuclides should be considered.

2.2.1. Radiolabeling. BnDTPA-EphA2-230-1 was labeled with [^{111}In]In (Figure 2). As a result, [^{111}In]In-BnDTPA-EphA2-230-1 was obtained at an 83.6% (5.1 MBq/100 μg) radiochemical yield and high radiochemical purity (98.5%; Figure S2).

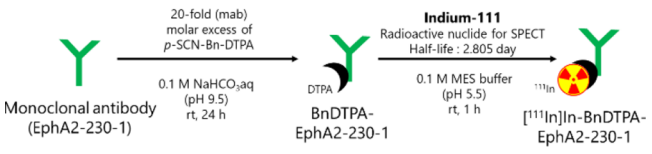

Figure 2. Scheme of the labeling of [^{111}In]In-BnDTPA-EphA2-230-1.

2.3. Cell-Binding Study. The uptake of [^{111}In]In-BnDTPA-EphA2-230-1 in U87MG cells is shown in Figure 3. The cellular uptake of [^{111}In]In-BnDTPA-EphA2-230-1

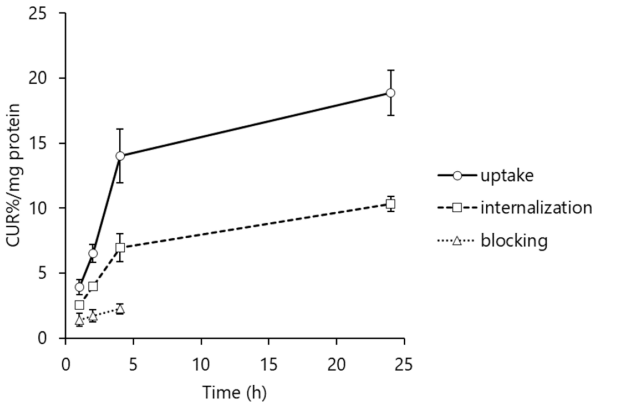

Figure 3. Results of cell-binding assay. [^{111}In]In-BnDTPA-EphA2-230-1 (3.7 kBq/0.4 μg) was incubated with U87MG cells at 37 °C for various time periods. In the internalization group, the U87MG cells were washed with acid buffer (0.2 M CH_3COOH, 0.5 M NaCl). In the blocking group, [^{111}In]In-BnDTPA-EphA2-230-1 and nonlabeled EphA2-230-1 (6.25 μg) were incubated with U87MG cells.

increased in a time-dependent manner (cellular uptake ratio [CUR], 14.0 ± 2.1%/mg protein at 4 h). In contrast, the CUR of [^{111}In]In-BnDTPA-EphA2-230-1 significantly decreased by the addition of the EphA2-230-1 antibody (90.9% reduction at 4 h). The intracellular uptake ratio was 10.3 ± 0.6%/mg protein at 24 h, which corresponds to 54.8% of the total cellular uptake at 24 h. As a result, [^{111}In]In-BnDTPA-EphA2-230-1 was shown to be taken up into U87MG cells in a time-dependent manner. On the other hand, [^{111}In]In-BnDTPA-EphA2-230-1 was barely taken up into the cells in the blocking group at 4 h. This cold-target inhibition assay demonstrates that the cellular uptake of [^{111}In]In-BnDTPA-EphA2-230-1 is mediated by EphA2 but not by nonspecific endocytosis in U87MG cells.

2.4. Biodistribution. Figure 4 summarizes the biodistribution results of [^{111}In]In-BnDTPA-EphA2-230-1 in U87MG tumors after intravenous injection of [^{111}In]In-BnDTPA-EphA2-230-1 (37 kBq/1.2 μg/100 μL saline). The time-course uptake of [^{111}In]In-BnDTPA-EphA2-230-1 in the

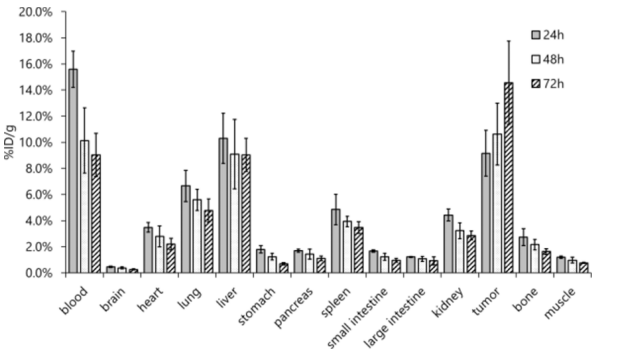

Figure 4. Biodistribution results in U87MG tumor-bearing mice. Biodistribution of [^{111}In]In-BnDTPA-EphA2-230-1 in U87MG tumor-bearing mice 24, 48, and 72 h after injection in normal tissues and tumor. Data are represented as the mean ± standard deviation (SD); n = 4.

https://doi.org/10.1021/acsomega.2c07849
ACS Omega 2023, 8, 7030−7035

tissues of U87MG tumor-bearing mice is presented as the percent of the injected dose per gram of tissue (% ID/g) shown in Figure 4. The uptake of [^{111}In]In-BnDTPA-EphA2-230-1 by the experimental tumors reached 14.6 ± 3.2% ID/g 72 h post-injection. In addition, uptake was observed in the liver (9.0 ± 1.3% ID/g at 72 h) and spleen (3.5 ± 0.5% ID/g at 72 h). Overall, high uptake of [^{111}In]In-BnDTPA-EphA2-230-1 in the tumor was confirmed and continued to increase for 72 h. This indicates that tumors can be more clearly imaged by SPECT imaging using [^{111}In]In-BnDTPA-EphA2-230-1. In contrast, [^{111}In]In-BnDTPA-EphA2-230-1 showed nonspecific uptake in the liver, blood, and spleen. Uptake in these organs has also been found with imaging tracers using antibodies,[19,25,26] but uptake in the liver was particularly high. The uptake of [^{111}In]In-BnDTPA-EphA2-230-1 was increased in the liver, since EphA2 is expressed in the liver.[27] Table 1 shows

Table 1. Tumor-to-Blood and Tumor-to-Muscle Ratios

	time after injection (h)		
ratio	24	48	72
tumor-to-blood	0.6 ± 0.1	1.1 ± 0.1	1.7 ± 0.6
tumor-to-muscle	7.6 ± 1.3	11.0 ± 1.1	19.2 ± 4.6

the tumor-to-muscle and tumor-to-blood ratios for each time point. Both ratios increased over time and more than doubled 72 h after injection (tumor-to-blood = 1.7-fold at 72 h, tumor-to-muscle = 19.2-fold at 72 h; Table 1). Finally, [^{111}In]In-BnDTPA-EphA2-230-1 exhibited a tumor-to-blood ratio superior to that previously reported ^{111}In-CHX-A"-DTPA-DS-8895a at an earlier time point ([^{111}In]In-BnDTPA-EphA2-230-1 = 1.7 at 72 h, ^{111}In-CHX-A"-DTPA-DS-8895a = 0.94 at 7 d).[19]

2.5. Blocking Biodistribution. We performed a blocking biodistribution study. For biodistribution under EphA2 blocking conditions, 10 mg/kg of EphA2-230-1 in 100 μL of saline was injected intravenously 24 h before the intravenous injection of [^{111}In]In-BnDTPA-EphA2-230-1 (37 kBq/1.2 μg/100 μL saline). The uptake of [^{111}In]In-BnDTPA-EphA2-230-1 in tumors was reduced in the blocking group compared to the control group (control: 14.6 ± 3.2% ID/g, blocking: 6.3 ± 2.5% ID/g at 72 h; Figure S3). Figure 5 shows the tumor-to-muscle and tumor-to-blood ratios at 72 h in the control and blocking groups. Both ratios were significantly reduced in the blocking group compared to the control group (tumor-to-blood, control: 1.7 ± 0.6, blocking: 0.6 ± 0.1 at 72 h, 64.7% reduction; tumor-to-muscle, control: 19.2 ± 4.6, blocking: 6.8 ± 1.2 at 72 h, 64.6% reduction).

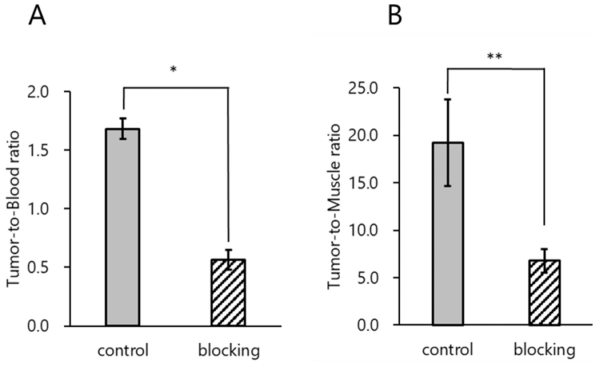

Figure 5. Tumor-to-blood ratio (A) and tumor-to-muscle ratio (B) in control and blocking groups. Data are represented as the mean ± SD; n = 4. *:p < 0.05, **:p < 0.01 by Student's t test.

2.6. SPECT/CT. SPECT/CT imaging was conducted in U87MG tumor-bearing mice 72 h after intravenous administration of 7.2 MBq/114 μg of [^{111}In]In-BnDTPA-EphA2-230-1 in 120 μL of saline. A 5 min CT scan on an X-CUBE scanner (MOLECUBES, Ghent, Belgium) was initially performed for attenuation correction followed by a 60 min SPECT scan on a γ-CUBE scanner (MOLECUBES). SPECT/CT imaging was conducted in U87MG tumor-bearing mice 72 h after intravenous administration of [^{111}In]In-BnDTPA-EphA2-230-1. As shown in Figure 6A,B, the implanted

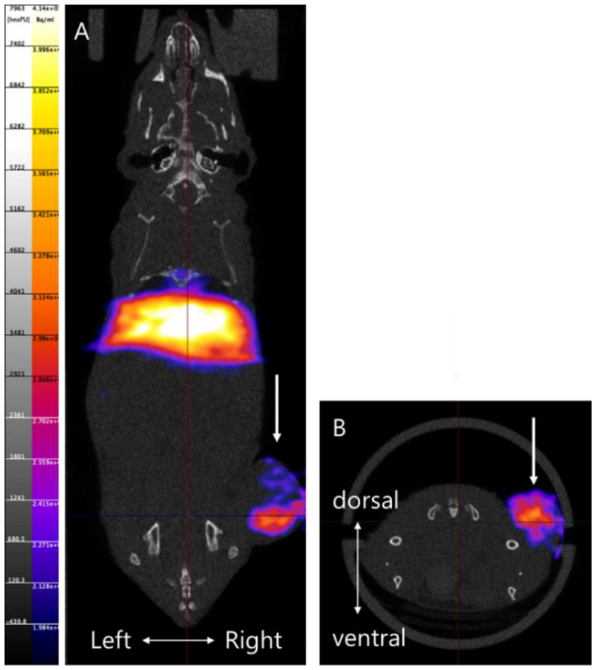

Figure 6. SPECT imaging of U87MG tumor-bearing mouse. Representative [^{111}In]In-BnDTPA-EphA2-230-1 SPECT/CT imaging in U87MG tumor-bearing mouse 72 h after injection. Dorsal view (A) and caudal view (B). The tumor is indicated by the arrows.

U87MG tumors in the right limbs were clearly visualized (Figure S4). However, in SPECT images, the liver and tumor could be clearly visualized. This is a reasonable result when the organ weights are taken into account based on the results of the biodistribution study (Figure S5).

3. CONCLUSIONS

This study evaluated the affinity and pharmacokinetics of a novel monoclonal antibody, [^{111}In]In-BnDTPA-EphA2-230-1, targeting EphA2. [^{111}In]In-BnDTPA-EphA2-230-1 specifically bound to EphA2s expressed in tumors. Biodistribution analysis showed that [^{111}In]In-BnDTPA-EphA2-230-1 exhibited high tumor accumulation. In addition, the tumor-to-blood ratio was superior to that previously reported for ^{111}In-CHX-A"-DTPA-DS-8895a. Finally, a U87MG tumor implanted in the right limb of a mouse was clearly visualized via SPECT imaging. Consequently, [^{111}In]In-BnDTPA-EphA2-230-1 can be considered as a potential imaging tracer for EphA2.

https://doi.org/10.1021/acsomega.2c07849
ACS Omega 2023, 8, 7030−7035

4. EXPERIMENTAL PROCEDURES

4.1. General. Mouse monoclonal antibody against human EphA2 termed EphA2-230-1 was provided by co-author Kazunori Kato. Additionally, *p*-SCN-Bn-DTPA was purchased from Macrocyclics, Inc. (Plano, TX, USA), and 2-(N-morpholino)ethanesulfonic acid (MES) was purchased from Sigma-Aldrich (St. Louis, MO, USA). [^{111}In]$InCl_3$ was purchased from Nihon Medi-Physics Co. Ltd. (Tokyo, Japan). Most chemicals were purchased from Tokyo Chemical Industry Co., Ltd. (TCI) (Tokyo, Japan), Nacalai Tesque Inc. (Kyoto, Japan), and Fujifilm Wako Pure Chemical Corporation (Osaka, Japan) and used without further purification.

4.2. DTPA Conjugates with the Antibody. EphA2-230-1 (200 μg) was diluted in 0.1 M $NaHCO_3$ (pH 9.5, 30 μL), then added to a 20-fold molar excess of p-SCN-Bn-DTPA diluted in 0.1 M $NaHCO_3$ (pH 9.5, 30 μL), and mixed at room temperature for 24 h. The reaction mixture was then purified by gel filtration chromatography using PD-10 (GE healthcare, Little Chalfont, UK), and the appropriate fractions were collected and concentrated using a centrifugal filter (Amicon Ultra 0.5 mL, Ultracel-100 K, Merck, Darmstadt, Germany). We observed the reaction progress using MALDI-TOF-MS. 3,5-Dimethoxy-4-hydrocinnamic acid (TCI) was saturated with 0.1% trifluoroacetic acid solution/acetonitrile (1:1). The antibody was dissolved in this aqueous solution and measured.

4.3. Flow Cytometry Measurement of Binding Affinity for EphA2. The reactivity of EphA2-230-1, BnDTPA-EphA2-230-1, and natIn-BnDTPA-EphA2-230-1 to EphA2 on the cancer cell surface was determined using flow cytometry. Approximately 1 × 10^5 U87MG cells were incubated with various concentrations (1.6−100 μg/mL) of antibody in 20 μL of phosphate-buffered saline (PBS; pH 7.4) with 2% fetal bovine serum (FBS; staining buffer) for 60 min on ice. The cells were then washed and stained with the phycoerythrin-conjugated goat anti-mouse IgG secondary antibody (Invitrogen, Waltham, MA, USA) for 30 min on ice. The cell suspension was washed three times with PBS and then analyzed using a FACSCalibur flow cytometer (BD Immunocytometry Systems, Franklin Lakes, NJ, USA). Equilibrium dissociation constants were calculated using GraphPad Prism 6 (GraphPad Software, San Diwgo, CA, USA).

4.4. Radiolabeling. BnDTPA-EphA2-230-1 (100 μg) was diluted in 0.1 M MES buffer (pH 5.5, 200 μL) and then added to [^{111}In]$InCl_3$ (6.1 MBq) and mixed at room temperature for 1 h. After the reaction, the reaction mixture was concentrated and purified using a centrifugal filter (Amicon Ultra 0.5 mL, Ultracel-100 K). Purified [^{111}In]In-BnDTPA-EphA2-230-1 was analyzed using radio-thin-layer chromatography (TLC; 25 Aluminium TLC silicagel 60 F254, Merck) with saturated ethylenediaminetetraacetic acid solution. Autoradiography was carried out using a Typhoon FLA 9500 BGR (GE healthcare).

4.5. Cell Culture. The U87MG glioma cell line was obtained from the European Collection of Authenticated Cell Cultures (London, UK). The cells were grown in Eagle's minimal essential medium (Fujifilm Wako Pure Chemical Corporation) supplemented with 10% FBS (Sigma-Aldrich), 2 mM L-glutamine (Nacalai Tesque Inc.), 1 mM pyruvic acid (Nacalai Tesque Inc.), nonessential amino acid (Nacalai Tesque Inc.), and penicillin−streptomycin (Nacalai Tesque Inc.). The cells were cultured under 5% CO_2 and 95% ambient air at 37 °C.

4.6. Cell-Binding Study. *4.6.1. Uptake of [^{111}In]In-BnDTPA-EphA2-230-1.* The U87MG cells (approximately 5 × 10^4/well) were seeded in a 24-well cell culture plate (Corning, Corning, NY, USA) containing a growth medium and incubated at 37 °C under 5% CO_2 until 80% confluence was achieved. The medium was aspirated and replaced with 1.5 mL of the FBS-free medium. After 10 min, the cells were treated with [^{111}In]In-BnDTPA-EphA2-230-1 (3.7 kBq/0.4 μg). After 1, 2, 4, and 24 h of additional incubation, the radioactive medium was aspirated, and the plate was washed twice with 0.5 mL of cold PBS. After washing, the cellular fraction was lysed with 0.1 M NaOH, and the protein concentration was calculated using a BCA Protein Assay Kit (Thermo Fisher Scientific, Waltham, MA, USA). Radioactivity counts containing the radioactive medium and PBS were designated as Cout, and radioactivity counts of the lysis solution and PBS were defined as Cin. The radioactivity of each fraction was measured using a γ-counter (1480 Automatic Gamma Counter, Perkin Elmer, Waltham, MA, USA). CUR was calculated using the formula Cin/(Cin + Cout).

4.6.2. Internalization of [^{111}In]In-BnDTPA-EphA2-230-1. The procedure of cell culture was the same as that described above. The medium was aspirated and replaced with 1.5 mL of the FBS-free medium. After 10 min, the cells were treated with [^{111}In]In-BnDTPA-EphA2-230-1 (3.7 kBq/0.4 μg). After 1, 2, 4, and 24 h of additional incubation, the radioactive medium was aspirated, and the plate was washed twice with 0.5 mL of cold PBS. After washing, the cells were washed three times with acid buffer (0.2 M CH_3COOH, 0.5 M NaCl). Finally, the cellular fraction was lysed with 0.1 M NaOH, and the protein concentration was calculated using a BCA Protein Assay Kit. The radioactivity was defined, measured, and calculated as described in the previous sections.

4.6.3. Blocking of [^{111}In]In-BnDTPA-EphA2-230-1. The procedure of cell culture was the same as that described above. The medium was aspirated and replaced with 1.0 mL of FBS-free medium followed by 0.5 mL of FBS-free medium with unlabeled EphA2-230-1 (6.25 μg) to determine nonspecific binding. After 10 min, the cells were cotreated with [^{111}In]In-BnDTPA-EphA2-230-1 (3.7 kBq/0.4 μg) and EphA2-230-1 (6.25 μg). After 1, 2, and 4 h of additional incubation, the radioactive medium was aspirated, and the plate was washed twice with 0.5 mL of cold PBS. After washing, the cellular fraction was lysed with 0.1 M NaOH, and the protein concentration was calculated using a BCA Protein Assay Kit. The radioactivity was defined, measured, and calculated as described in the previous sections.

4.7. Animal Model. The animal studies were approved by the Bioscience Research Center at Kyoto Pharmaceutical University and performed according to the Guidelines for Animal Experimentation. Five-week-old male BALB/c Slc-nu/nu mice were obtained from Japan SLC (Shizuoka, Japan). For each mouse, 2 × 10^6 U87MG glioblastoma cells in 100 μL PBS were inoculated subcutaneously into the right thigh. The tumor reached an approximate volume of 100 mm^3 after 28−35 days. The mice were then used for biodistribution analysis and SPECT/CT imaging.

4.8. Biodistribution. Biodistribution analysis was conducted in U87MG tumor-bearing mice. [^{111}In]In-BnDTPA-EphA2-230-1 (37 kBq/1.2 μg/100 μL saline) was administered to the mice intravenously through the tail vein. At 24, 48, and 72 h after administration, the mice were euthanized by exsanguination. The blood, brain, heart, lung, liver, pancreas,

https://doi.org/10.1021/acsomega.2c07849
ACS Omega 2023, 8, 7030−7035

spleen, kidneys, stomach, intestines (small and large), skeletal muscles, bones, and tumors were removed for analysis. The tissue samples were weighed, and radioactivity was determined. Tissue radioactivity levels were expressed as % ID/g.

4.9. Blocking Biodistribution. Blocking biodistribution analysis was conducted in U87MG tumor-bearing mice. [^{111}In]In-BnDTPA-EphA2-230-1 (37 kBq/1.2 μg/100 μL saline) was administered to the mice intravenously through the tail vein. For biodistribution under EphA2 blocking conditions, 10 mg/kg of EphA2-230-1 in 100 μL saline was injected intravenously 24 h before the radiotracer injection. At 72 h after tracer administration, the mice were euthanized by exsanguination. The blood, brain, heart, lung, liver, pancreas, spleen, kidneys, stomach, intestines (small and large), skeletal muscle, bone, and tumor were removed for analysis. The tissue samples were weighed, and radioactivity was determined. The tissue radioactivity levels were expressed as described in the previous section.

4.10. SPECT/CT. For the bolus injection study, tumor-bearing mice were intravenously injected with 7.2 MBq/114 μg [^{111}In]In-BnDTPA-EphA2-230-1 in 120 μL of saline. SPECT/CT images were obtained using X-CUBE and γ-CUBE scanners. The mice were anesthetized using isoflurane/O_2 (5% for induction, 2.5% for maintenance), and their body temperature was kept constant with an integrated heating circuit. At 72 h after administration, CT imaging was performed for 5 min, and SPECT imaging was performed for 60 min after CT imaging. The SPECT images were acquired using a helical-orbit scan with linear-stage motion and step-and-shoot camera motion. A multi-lofthole collimator (GPmouse, 48 loftholes) was mounted in a heptagonal SPECT system, and the following parameters were used: [^{111}In]In energy window (26 keV ± 10%, 171 keV ± 10%, and 245 keV ± 10%), 237 projections, 18° angle increment with a 1 mm bed step, and 60 min acquisition time. SPECT projection data were reconstructed using a 3D maximum likelihood-expectation maximization algorithm (3 iterations) at an isotropic voxel size of 250 μm. CT images were subsequently acquired using a helical scan with the following acquisition parameters: X-ray source setting of 50 kVp/100 μA, 480 projections, 1.4 spiral pitch, and 1 min acquisition time. CT projections were reconstructed using an ISRA algorithm that yielded a 0.2 mm × 0.2 mm × 0.2 mm voxel size and 200 × 220 × 469 image volume. Image analysis was performed using the VivoQuant software (version 4.0 patch1, inviCRO, LLC, Boston, MA, USA).

4.11. Statistics. Student's *t* test was performed for blocking distribution using XLSTAT (Addinsoft, New York, NY, USA). The data points represent the mean of at least triplicate measurements with error bars corresponding to the SD.

■ ASSOCIATED CONTENT

Supporting Information

The Supporting Information is available free of charge at https://pubs.acs.org/doi/10.1021/acsomega.2c07849.

Molecular weights of EphA2-230-1 and BnDTPA-EphA2-230-1 using MALDI-TOF; analysis of [^{111}In]In-BnDTPA-EphA2-230-1; biodistribution result in U87MG tumor-bearing mice; SPECT tomogram of Figure 6 reconstructed into a 3D image; and liver and tumor uptake results for biodistribution in U87MG tumor-bearing mice 72 h post-injection, converted to % ID (PDF)

■ AUTHOR INFORMATION

Corresponding Author

Hiroyuki Kimura − *Department of Analytical and Bioinorganic Chemistry, Division of Analytical and Physical Science, Kyoto Pharmaceutical University, Kyoto 607-8414, Japan*; orcid.org/0000-0002-4291-3524; Phone: +81-75-595-4630; Email: hkimura@mb.kyoto-phu.ac.jp; Fax: +81-75-595-4753

Authors

Takenori Furukawa − *Department of Analytical and Bioinorganic Chemistry, Division of Analytical and Physical Science, Kyoto Pharmaceutical University, Kyoto 607-8414, Japan*

Minon Sasaki − *Department of Analytical and Bioinorganic Chemistry, Division of Analytical and Physical Science, Kyoto Pharmaceutical University, Kyoto 607-8414, Japan*

Takumu Yamada − *Department of Biomedical Engineering, Faculty of Science and Engineering, Toyo University, Saitama 350-0815, Japan*

Takumi Iwasawa − *Department of Biomedical Engineering, Faculty of Science and Engineering, Toyo University, Saitama 350-0815, Japan*

Yusuke Yagi − *Department of Analytical and Bioinorganic Chemistry, Division of Analytical and Physical Science, Kyoto Pharmaceutical University, Kyoto 607-8414, Japan; Department of Radiological Technology, Faculty of Medicinal Science, Kyoto College of Medical Science, Kyoto 622-0022, Japan*

Kazunori Kato − *Department of Biomedical Engineering, Faculty of Science and Engineering, Toyo University, Saitama 350-0815, Japan*

Hiroyuki Yasui − *Department of Analytical and Bioinorganic Chemistry, Division of Analytical and Physical Science, Kyoto Pharmaceutical University, Kyoto 607-8414, Japan*

Complete contact information is available at: https://pubs.acs.org/10.1021/acsomega.2c07849

Funding

This work was supported by JSPS KAKENHI (grant number: JP22H02928).

Notes

The authors declare no competing financial interest.

■ ABBREVIATIONS

CUR, cellular uptake ratio; CT, computed tomography; DTPA, diethylenetriamine pentaacetic acid; Eph, erythropoietin-producing hepatocellular; EphA2, erythropoietin-producing hepatocellular receptor A2; EphA2-230-1, EphA2-230-1 monoclonal antibody; FBS, fetal bovine serum; MALDI-TOF-MS, matrix-assisted laser desorption/ionization time-of-flight mass spectrometry; MES, 2-(N-morpholino)-ethanesulfonic acid; % ID/g, percent of the injected dose per gram of tissue; PBS, phosphate-buffered saline; *p*-SCN-Bn-DTPA, 2-(4-isothiocyanatobenzyl)-diethylenetriaminepenta-acetic acid; SD, standard deviation; SPECT, single-photon emission computed tomography

https://doi.org/10.1021/acsomega.2c07849
ACS Omega 2023, 8, 7030−7035

REFERENCES

(1) Gale, N. W.; Yancopoulos, G. D. Ephrins and Their Receptors: a Repulsive Topic? *Cell Tissue Res.* **1997**, *290*, 227−241.

(2) Miao, H.; Wang, B. Eph/Ephrin Signaling in Epithelial Development and Homeostasis. *Int. J. Biochem. Cell Biol.* **2009**, *41*, 762−770.

(3) Zhou, Y.; Sakurai, H. Emerging and Diverse Functions of the EphA2 Noncanonical Pathway in Cancer Progression. *Biol. Pharm. Bull.* **2017**, *40*, 1616−1624.

(4) Pasquale, E. B. Eph-Ephrin Bidirectional Signaling in Physiology and Disease. *Cell* **2008**, *133*, 38−52.

(5) Pasquale, E. B. Eph Receptors and Ephrins in Cancer: Bidirectional Signalling and Beyond. *Nat. Rev. Cancer* **2010**, *10*, 165−180.

(6) Miao, H.; Li, D. Q.; Mukherjee, A.; Guo, H.; Petty, A.; Cutter, J.; Basilion, J. P.; Sedor, J.; Wu, J.; Danielpour, D.; Sloan, A. E.; Cohen, M. L.; Wang, B. EphA2 Mediates Ligand-Dependent Inhibition and Ligand-Independent Promotion of Cell Migration and Invasion via a Reciprocal Regulatory Loop With Akt. *Cancer Cell* **2009**, *16*, 9−20.

(7) Huang, F.; Reeves, K.; Han, X.; Fairchild, C.; Platero, S.; Wong, T. W.; Lee, F.; Shaw, P.; Clark, E. Identification of Candidate Molecular Markers Predicting Sensitivity in Solid Tumors to Dasatinib: Rationale for Patient Selection. *Cancer Res.* **2007**, *67*, 2226−2238.

(8) Wang, X. D.; Reeves, K.; Luo, F. R.; Xu, L. A.; Lee, F.; Clark, E.; Huang, F. Identification of Candidate Predictive and Surrogate Molecular Markers for Dasatinib in Prostate Cancer: Rationale for Patient Selection and Efficacy Monitoring. *Genome Biol.* **2007**, *8*, R255.

(9) Tandon, M.; Vemula, S. V.; Mittal, S. K. Emerging Strategies for EphA2 Receptor Targeting for Cancer Therapeutics. *Expert Opin. Ther. Targets* **2011**, *15*, 31−51.

(10) Zelinski, D. P.; Zantek, N. D.; Stewart, J. C.; Irizarry, A. R.; Kinch, M. S. EphA2 Overexpression Causes Tumorigenesis of Mammary Epithelial Cells. *Cancer Res.* **2001**, *61*, 2301−2306.

(11) Macrae, M.; Neve, R. M.; Rodriguez-Viciana, P.; Haqq, C.; Yeh, J.; Chen, C.; Gray, J. W.; McCormick, F. A Conditional Feedback Loop Regulates Ras Activity Through EphA2. *Cancer Cell* **2005**, *8*, 111−118.

(12) Nikas, I.; Giaginis, C.; Petrouska, K.; Alexandrou, P.; Michail, A.; Sarantis, P.; Tsourouflis, G.; Danas, E.; Pergaris, A.; Politis, P. K.; Nakopoulou, L.; Theocharis, S. EPHA2, EPHA4, and EPHA7 Expression in Triple-Negative Breast Cancer. *Diagnostics* **2022**, *12*, 366.

(13) Kamoun, W. S.; Dugast, A. S.; Suchy, J. J.; Grabow, S.; Fulton, R. B.; Sampson, J. F.; Luus, L.; Santiago, M.; Koshkaryev, A.; Sun, G.; Askoxylakis, V.; Tam, E.; Huang, Z. R.; Drummond, D. C.; Sawyer, A. J. Synergy Between EphA2-ILs-DTXp, a Novel EphA2-Targeted Nanoliposomal Taxane, and PD-1 Inhibitors in Preclinical Tumor Models. *Mol. Cancer Ther.* **2020**, *19*, 270−281.

(14) Shi, H.; Yu, F.; Mao, Y.; Ju, Q.; Wu, Y.; Bai, W.; Wang, P.; Xu, R.; Jiang, M.; Shi, J. EphA2 Chimeric Antigen Receptor-Modified T Cells for the Immunotherapy of Esophageal Squamous Cell Carcinoma. *J. Thorac. Dis.* **2018**, *10*, 2779−2788.

(15) Amato, K. R.; Wang, S.; Hastings, A. K.; Youngblood, V. M.; Santapuram, P. R.; Chen, H.; Cates, J. M.; Colvin, D. C.; Ye, F.; Brantley-Sieders, D. M.; Cook, R. S.; Tan, L.; Gray, N. S.; Chen, J. Genetic and Pharmacologic Inhibition of EPHA2 Promotes Apoptosis in NSCLC. *J. Clin. Invest.* **2014**, *124*, 2037−2049.

(16) Cai, W.; Ebrahimnejad, A.; Chen, K.; Cao, Q.; Li, Z. B.; Tice, D. A.; Chen, X. Quantitative radioimmunoPET Imaging of EphA2 in Tumor-Bearing Mice. *Eur. J. Nucl. Med. Mol. Imaging* **2007**, *34*, 2024−2036.

(17) Jackson, D.; Gooya, J.; Mao, S.; Kinneer, K.; Xu, L.; Camara, M.; Fazenbaker, C.; Fleming, R.; Swamynathan, S.; Meyer, D.; Senter, P. D.; Gao, C.; Wu, H.; Kinch, M.; Coats, S.; Kiener, P. A.; Tice, D. A. A Human Antibody-Drug Conjugate Targeting EphA2 Inhibits Tumor Growth In Vivo. *Cancer Res.* **2008**, *68*, 9367−9374.

(18) Jacobson, O.; Li, Q.; Chen, H.; Niu, G.; Kiesewetter, D. O.; Xu, L.; Cook, K.; Yang, G.; Dall'Acqua, W.; Tsui, P.; Peng, L.; Chen, X. PET-Guided Evaluation and Optimization of Internalized Antibody−Drug Conjugates Targeting Erythropoietin-Producing Hepatoma A2 Receptor. *J. Nucl. Med.* **2017**, *58*, 1838−1844.

(19) Burvenich, I. J. G.; Parakh, S.; Gan, H. K.; Lee, F. T.; Guo, N.; Rigopoulos, A.; Lee, S. T.; Gong, S.; O'Keefe, G. J.; Tochon-Danguy, H.; Kotsuma, M.; Hasegawa, J.; Senaldi, G.; Scott, A. M. Molecular Imaging and Quantitation of EphA2 Expression in Xenograft Models With 89Zr-DS-8895a. *J. Nucl. Med.* **2016**, *57*, 974−980.

(20) Sakamoto, A.; Kato, K.; Hasegawa, T.; Ikeda, S. An Agonistic Antibody to EPHA2 Exhibits Antitumor Effects on Human Melanoma Cells. *Anticancer Res.* **2018**, *38*, 3273−3282.

(21) Shitara, K.; Satoh, T.; Iwasa, S.; Yamaguchi, K.; Muro, K.; Komatsu, Y.; Nishina, T.; Esaki, T.; Hasegawa, J.; Kakurai, Y.; Kamiyama, E.; Nakata, T.; Nakamura, K.; Sakaki, H.; Hyodo, I. Safety, Tolerability, Pharmacokinetics, and Pharmacodynamics of the Afucosylated, Humanized Anti-EPHA2 Antibody DS-8895a: a First-in-Human Phase I Dose Escalation and Dose Expansion Study in Patients With Advanced Solid Tumors. *J. Immunother. Cancer* **2019**, *7*, 219.

(22) Murakoshi, M.; Iwasawa, T.; Koshida, T.; Suzuki, Y.; Gohda, T.; Kato, K. Development of an In-House EphA2 ELISA for Human Serum and Measurement of Circulating Levels of EphA2 in Hypertensive Patients with Renal Dysfunction. *Diagnostics* **2022**, *12*, 3023.

(23) Kato, K.; Agatsuma, T.; Hasegawa, J. Anti-EphA2 Antibody and Immunological Detection of EphA2 Using Same. Patent Number WO2018135653A1.

(24) Furukawa, T.; Kimura, H.; Torimoto, H.; Yagi, Y.; Kawashima, H.; Arimitsu, K.; Yasui, H. A Putative Single-Photon Emission CT Imaging Tracer for Erythropoietin-Producing Hepatocellular A2 Receptor. *ACS Med. Chem. Lett.* **2021**, *12*, 1238−1244.

(25) Veal, M.; Dias, G.; Kersemans, V.; Sneddon, D.; Faulkner, S.; Cornelissen, B. A Model System to Explore the Detection Limits of Antibody-Based Immuno-SPECT Imaging of Exclusively Intranuclear Epitopes. *J. Nucl. Med.* **2021**, *62*, 1537−1544.

(26) Solomon, V. R.; Alizadeh, E.; Bernhard, W.; Hartimath, S. V.; Hill, W.; Chekol, R.; Barreto, K. M.; Geyer, C. R.; Fonge, H. 111 In- and 225 Ac-Labeled Cixutumumab for Imaging and α-Particle Radiotherapy of IGF-1R Positive Triple-Negative Breast Cancer. *Mol. Pharmaceutics* **2019**, *16*, 4807−4816.

(27) Kaushansky, A.; Douglass, A. N.; Arang, N.; Vigdorovich, V.; Dambrauskas, N.; Kain, H. S.; Austin, L. S.; Sather, D. N.; Kappe, S. H. I. Malaria Parasites Target the Hepatocyte Receptor EphA2 for Successful Host Infection. *Science* **2015**, *350*, 1089−1092.

https://doi.org/10.1021/acsomega.2c07849
ACS Omega 2023, 8, 7030−7035